

# Automatic Respiratory Gating for Contrast Ultrasound Evaluation of Liver Lesions

Damianos Christofides, *Student Member, IEEE*, Edward Leen,  
and Michalakis A. Averkiou, *Senior Member, IEEE*

**Abstract**—Dynamic contrast-enhanced ultrasound (DCEUS) has been used in radiology for many years for lesion detection and characterization. In recent years, more emphasis has been placed on tumor perfusion quantification with DCEUS. To ensure accuracy in both quantitative and qualitative evaluation of liver tumors with DCEUS, sources of noise in clinical data must be identified and, if possible, removed. One of the major sources of such noise is respiratory motion. A new automatic respiratory gating (ARG) algorithm is presented and evaluated with clinical data. The results of the evaluation demonstrate the potential of the ARG algorithm for clinical use as a fast and easy-to-implement method for removing respiratory motion from DCEUS loops.

## I. INTRODUCTION

MICROBUBBLES have been used in medical ultrasound imaging since the mid-1990s [1]. Microbubbles have the advantage of being a pure blood-pool contrast agent because they are similar in size to red blood cells [2], [3], allowing for the imaging of perfusion in real time. Ultrasound imaging with microbubbles or dynamic contrast-enhanced ultrasound (DCEUS) has found uses in the evaluation of response to treatment of liver metastases [4], the analysis of focal nodular hyperplasia in the liver [5], the detection of coronary disease [6], and the assessment of microvascular damage after a myocardial infarction [7].

Quantification of DCEUS image loops provides important blood flow information on tumor microcirculation [8]. One of the biggest challenges in quantitative DCEUS for liver lesions is motion caused by respiration. Respiratory motion can cause the lesion, as it appears in the imaging plane, to change in size, shape, and location (Fig. 1). This causes problems in the qualitative evaluation of the lesion, because the clinician needs to take into account the movement of the lesion to evaluate its size and perfusion patterns. This type of motion might also cause significant problems in the quantitative evaluation of the lesion's perfusion, because the lesion will be moving in and out of a region-of-interest (ROI) that samples the DCEUS mean linear intensity, thus introducing noise artifacts.

Various approaches have been used clinically to compensate for the effects of respiratory motion. One such

approach is directing the patient to hold his or her breath at a specific breathing cycle phase desired by the clinician or sonographer, but this technique applies only to patients that have the ability to perform a breath hold that can last more than 40 s; another disadvantage of this technique is that hemodynamics are affected during breath holds [9], [10]. Another technique for respiratory motion compensation found in the literature [4] is to identify the position of the diaphragm at a reference position and reject frames in which the diaphragm deviates from the reference position. This is also a post-processing technique (it is implemented after the acquisition of the ultrasound loop) and it relies on the operator's expertise to identify the brightest moving reflector.

Several computational techniques have been proposed in the literature that would allow for fully or semi-automated compensation of respiratory motion. Renault *et al.* [11] introduced a technique based on independent component analysis (ICA) with which the respiratory cycle could be extracted manually from the ICA-derived components that represent motion; a threshold can be used on the final respiratory kinetics curve to derive the frames that belong to the end phases of the respiratory cycle. Mulé *et al.* [12] used principal component analysis (PCA) to extract the respiratory kinetics to perform fully automatic gating. A drawback of both these techniques is that, because the ultrasound acquisition is two-dimensional, there is uncertainty on the portion of the lesion, if any, that will be present at the extreme phases of the respiratory cycle, because of out-of-plane motion.

Rigid registration is another technique used to compensate for respiratory motion. Rognin *et al.* [13], [14] used a rigid registration technique, with 2-D translation and rotation, to realign frames to a reference frame; a disadvantage of this approach is that out-of-plane frames might be difficult, if not impossible, to re-align. Zhang *et al.* [15] also used rigid registration, with 2-D translation only, and frame selection to perform automatic gating; the algorithm rejected out-of-plane frames but it required a long computation time that would not be realistic in a clinical context. Both of these techniques require the user to manually draw ROI(s) on frames to denote the search space for the registration to take place.

In the present work, a new post-processing method is proposed for automatic respiratory gating (ARG) of dual-contrast imaging (an anatomical B-mode image and a contrast-specific image displayed side-by-side in the same frame) loops. The only input needed by the user is to select a trigger frame in which the lesion is clearly seen

Manuscript received May 28, 2013; accepted September 3, 2013.

D. Christofides and M. Averkiou are with the Department of Mechanical and Manufacturing Engineering, University of Cyprus, Nicosia, Cyprus (e-mail: maverk@ucy.ac.cy).

E. Leen is with the Imaging Department of Hammersmith Hospital, London, UK.

DOI <http://dx.doi.org/10.1109/TUFFC.2014.2876>

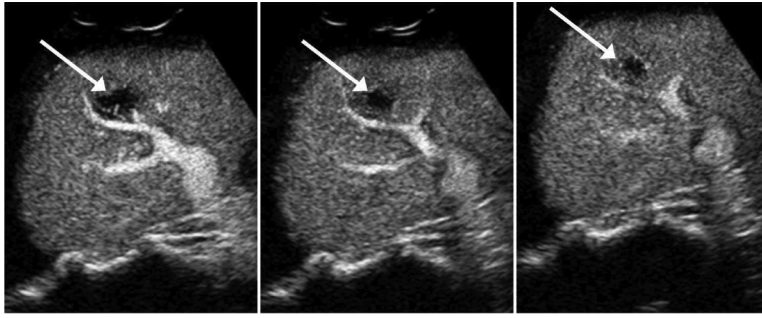


Fig. 1. Example of the changes of the size, location, and shape of a liver lesion, in a dynamic contrast-enhanced ultrasound (DCEUS) loop, at three different time instances. These changes are mainly attributed to respiratory motion.

and can be delineated. The new ARG algorithm is easy to implement and use, fast, and leads to a simple workflow for the clinical operator.

## II. MATERIALS AND METHODS

### A. ARG Algorithm

The ARG algorithm applies to the B-mode loop of the dual-contrast imaging loop acquisition because the anatomical information in the B-mode loop is less sensitive to intensity variation than the contrast loop. The algorithm is presented as implemented in this study, but modifications can be made to the algorithm to change its speed and/or performance. The software package Matlab (v. 2007b, The MathWorks Inc., Natick, MA) was used to implement the ARG algorithm.

1) *Quantify Amount of Motion*: Consider a B-mode loop consisting of  $N$  frames,  $\{I_i\}_{i=1}^N$ . First, the B-mode loop was downsampled by a factor of 2 (i.e., every other frame is kept) and resized using nearest-neighbor interpolation by a factor of 0.3. The resulting sequence of frames was stored as a new loop,  $\{\hat{I}_i\}_{i=1}^{\hat{N}}$ . To detect the motion present, each resulting frame was subtracted from the average of all the frames [16] (Fig. 2). The sequence of frames resulting from the subtraction is defined by

$$\{M_i\}_{i=1}^{\hat{N}} = \left\{ \hat{I}_i - \left( \frac{1}{\hat{N}} \sum_{i=1}^{\hat{N}} \hat{I}_i \right) \right\}_{i=1}^{\hat{N}}. \quad (1)$$

Next, the frames from  $\{M_i\}_{i=1}^{\hat{N}}$  were threshold to binary by the 30% of the maximum value of each frame. The result-

ing frames suffered from the presence of noise from single and small clusters of bright pixels present in the  $\{M_i\}_{i=1}^{\hat{N}}$  sequence. This problem was addressed by first removing single pixels from the thresholded binary images and then keeping only the  $n$  largest groups of clusters of connected pixels, called structures hereafter. The removal of single pixels was implemented using the morphological operation *clean* of the *bwmorph* function and the extraction of the largest structure using the *Area* operation of the *regionprops* function, both part of Matlab's Image Processing Toolbox. The sequential procedures of applying a threshold on the frames and the retention of the  $n$  largest structures will be referred to hereafter as image operator  $\mathfrak{S}$ . The  $\mathfrak{S}$  operator takes two arguments:  $X$ , which can be a frame or sequence of frames, and  $n$ , which is the number of largest structures that will be extracted by the operator. The  $\mathfrak{S}$  operator was applied on the  $\{M_i\}_{i=1}^{\hat{N}}$  sequence and the resulting binary frames were stored in the sequence  $\{P_i\}_{i=1}^{\hat{N}}$  (Fig. 3), according to

$$\{P_i\}_{i=1}^{\hat{N}} = \mathfrak{S}\{\{M_i\}_{i=1}^{\hat{N}}, n\}, \quad \text{with } n = 1. \quad (2)$$

Each frame from the  $\{P_i\}_{i=1}^{\hat{N}}$  sequence holds a moving structure extracted from the corresponding B-mode frame; thus, if all the frames from the  $\{P_i\}_{i=1}^{\hat{N}}$  sequence are added together, a map of the motion present in the whole B-mode loop can be produced. The result was a matrix made up of integer-value elements; each element in this matrix was associated with the amount of motion present at the corresponding pixel coordinate in the whole of the B-mode loop. This matrix was called the motion information matrix (MIM) (Fig. 4) and was calculated using

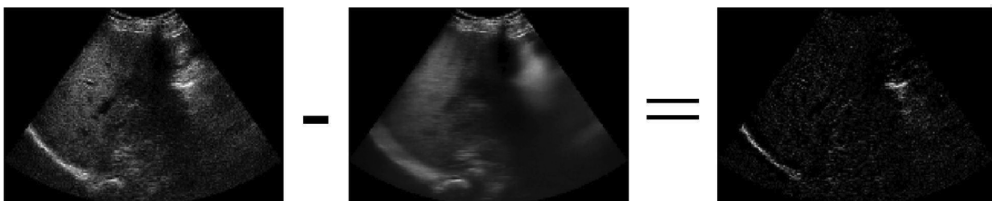


Fig. 2. Subtraction of a frame from the average of the  $\{\hat{I}_i\}_{i=1}^{\hat{N}}$  sequence. Note the relative increase of brightness of the diaphragm in the resulting frame compared with the original frame of the  $\{\hat{I}_i\}_{i=1}^{\hat{N}}$  sequence.

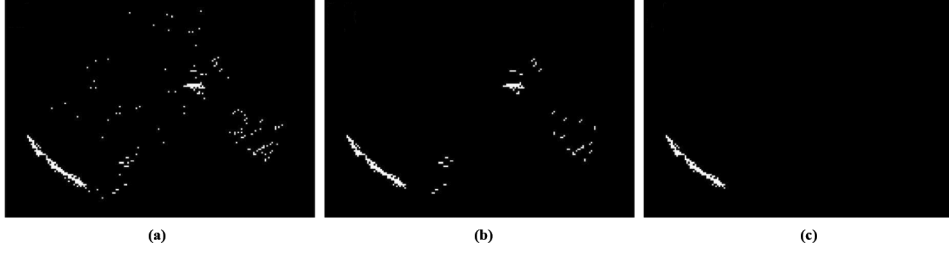


Fig. 3. Extraction of the largest moving structure from the  $\{M_i\}_{i=1}^{\hat{N}}$  sequence: (a) threshold image to binary by the 30% of the maximum pixel value, (b) remove single pixels, and (c) keep only first largest structure.

$$\text{MIM} = \sum \{P_i\}_{i=1}^{\hat{N}}. \quad (3)$$

2) *Establish Breathing Cycle to be Extracted:* As previously mentioned, the user must define the trigger frame before the ARG procedure begins. This frame defines the breathing cycle phase that was extracted by the ARG algorithm. First, the trigger frame was subtracted from the average of the uncompressed (without the reduction in the resolution)/undownsampling B-mode loop:

$$M_{\text{trigger}} = I_{\text{trigger}} - \frac{1}{N} \sum \{I_i\}_{i=1}^N. \quad (4)$$

The  $\mathfrak{S}$  image processing operator was then applied to the  $M_{\text{trigger}}$  frame according to

$$P_{\text{trigger}} = \mathfrak{S}(M_{\text{trigger}}, 5). \quad (5)$$

The MIM was resized to the original B-mode loop frame size using bicubic interpolation. The  $P_{\text{trigger}}$  frame's structures were overlaid over the MIM, and the mean intensity MIM value was calculated within each structure (Fig. 5). These values were stored in the  $\{S_M\}_{i=1}^5$  sequence, where the index  $i$  corresponds to each extracted structure.

The  $\{S_M\}_{i=1}^5$  sequence holds values of the amount of motion associated with each structure. This motion or change in the grayscale values of the B-mode loop frames could be due to respiration, cardiac motion, contrast agent presence, or any other change in the gray scale values of the B-mode loop through time.



Fig. 4. Example motion information matrix (MIM). Observe the two main areas in which motion occurs. The dominant structure producing motion is the diaphragm. Note that the values shown have been log-compressed to make the data easier to visualize.

In the interest of establishing whether the motion associated with each structure can be attributed to respiration, the mean grayscale intensity values for each frame of the B-mode loop within a square measuring  $30 \times 30$  pixels was calculated. The size of the square was selected by considering two competing factors: 1) the standard error of the mean of the grayscale intensity values decreases with the size of the square; and 2) a very large square would fail to detect motion from small moving structures. Based on these two factors, a  $30 \times 30$  square is optimal. The center of the square was placed at the center of mass of each structure of the  $P_{\text{trigger}}$  frame. Each structure on the  $P_{\text{trigger}}$  frame was identified by a specific index number assigned using the *bwlabel* function and the center of mass of each structure was calculated using the *Centroid* operation of the *regionprops* function, both part of Matlab's Image Processing Toolbox. This operation returned the time-intensity curve (TIC) associated with each extracted structure from the trigger frame. A square was used to extract the TIC, rather than using each structure as a binary mask, to reduce calculation time by approximately a factor of three. The next step was to calculate the Fourier transform (FT) of each TIC so its frequency contents could be analyzed (Fig. 6).

A metric was needed to quantify the presence the respiratory motion associated with each structure extracted from the trigger frame; these metric values were stored in the  $\{S_F\}_{i=1}^5$  sequence.  $\{S_F\}_{i=1}^5$  values were calculated as the area of the frequency spectrum between 0.1 and 0.5 Hz divided by the sum of the area from 0 to 0.1 Hz and the area between 0.5 to 1 Hz:

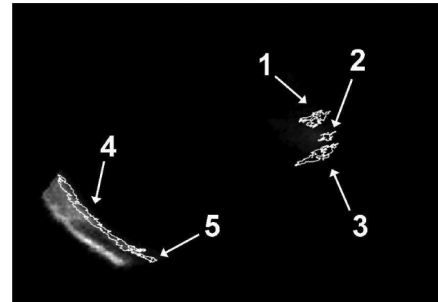


Fig. 5. Moving structures extracted from the trigger frame overlaid over the motion information matrix (MIM). The structures are labeled for reference purposes.

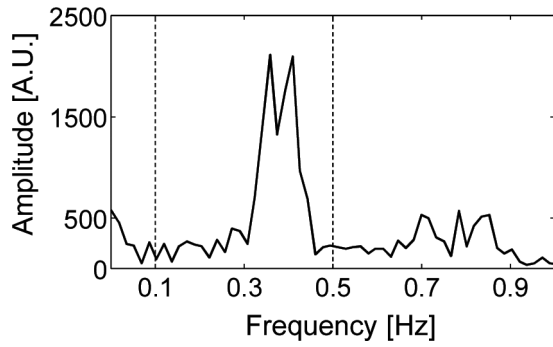


Fig. 6. The Fourier transform of the time-intensity curve (TIC) extracted from structure labeled 4 in Fig. 5. The respiration cycle bandwidth is denoted with the dashed vertical lines.

$$\{S_F\}_{i=1}^5 = \frac{\int_{0.1}^{0.5} F_i(f)df}{\int_0^{0.1} F_i(f)df + \int_{0.5}^1 F_i(f)df}. \quad (6)$$

The rationale for (6) is that the area between 0.1 and 0.5 Hz represents contributions to the frequency spectrum by respiration. The 0 to 0.1 Hz range represents contributions from slowly changing events, such as the change of grayscale values caused by the flow of microbubbles, and the 0.5 to 1 Hz frequency range represents sources of noise or physiological motion other than respiration present in the TIC curve. Thus, from (6), it can be observed that the values stored in  $\{S_F\}_{i=1}^5$  increase as respiratory motion presence increases and undesired change in grayscale values in the B-mode loop decreases.

Another metric that was recorded was whether the maximum value of the amplitude of the frequency spectrum lay within the respiration frequency range or not. This is a binary metric, stored in the  $\{S_B\}_{i=1}^5$  sequence, and it takes the values of either 0 or 1.

The combined metric, stored in the  $\{S\}_{i=1}^5$  sequence, is defined as

$$\{S\}_{i=1}^5 = \left( 0.6 \times \frac{\{S_M\}_{i=1}^5}{\max\{S_M\}_{i=1}^5} \right) + \left( 0.4 \times \frac{\{S_F\}_{i=1}^5}{\max\{S_F\}_{i=1}^5} \right). \quad (7)$$

Eq. (7) holds unless a structure receives an  $S_B$  of 0, then the corresponding  $S$  metric also receives a value of 0. If all the values  $\{S\}_{i=1}^5$  were given a zero value, then the  $\{S\}_{i=1}^5$  sequence reverted back to its original values before the consideration of  $S_B$ . In Table I, example  $\{S_M\}_{i=1}^5$ ,  $\{S_F\}_{i=1}^5$ ,  $\{S_B\}_{i=1}^5$ , and  $\{S\}_{i=1}^5$  values are shown for the structures in Fig. 5.

The TIC corresponding to the structure that receives the highest  $\{S\}_{i=1}^5$  score value was extracted again, this time using the structure as a binary mask applied on the B-mode loop. This was done to ensure maximum quality for the next step of the ARG procedure.

3) *Final Step of ARG Procedure:* The final step of the ARG procedure involves finding the location of the peaks

and troughs of the TIC of the structure that receives the highest  $S$  score. Peaks are indicative of the presence of a structure on the position it occupied on the trigger frame, whereas troughs indicate the absence of the structure from its position on the trigger frame. To locate the peaks of the TIC, the approximate time between the peaks of the TIC was calculated using the frequency spectrum. By locating the frequency at which the maximum amplitude occurs within the respiratory range (0.1 to 0.5 Hz),  $f_{\max}$ , the time between the peaks was approximated as  $T_{\max} = (f_{\max})^{-1}$ . The peaks were then located based on their separation being no less than  $T_{\max}/2$ ; this allows for flexibility because patient respiration frequency can fluctuate during examination. The location of the peaks was implemented by setting the parameter *MINPEAKDISTANCE* of Matlab's Signal Processing Toolbox *findpeaks* function to  $T_{\max}/2$ .

Once the peaks of the TIC were located, a piecewise cubic Hermite interpolating polynomial (pchip) was fitted on the peaks. The TIC was inverted and the same procedure was repeated to locate the troughs and fit a pchip on the troughs; thus, the envelope of the TIC was calculated. A threshold of 40% was then applied on the envelope of the signal and only frames that were above this threshold were accepted, the rest were rejected. The 40% value was established after considering the robustness of the fit of the lognormal model onto the data and at the same time optimizing the goodness of fit of the model. The frames that were accepted made up the ARG loop and were, within a threshold, at the same breathing cycle phase as the trigger frame (Fig. 7). The whole ARG algorithm is laid out in the flowchart shown in Fig. 8.

### B. Imaging Protocol

Eighteen (18) patients (7 female, 11 male) with liver metastasis were imaged. Approval for the scanning was obtained by the ethics review board of our hospital. The procedure was fully explained to all participating patients and informed consent was obtained.

All imaging was performed with a Philips iU22 scanner (Philips Medical Systems, Bothell, WA) using the C5-1 imaging probe. The imaging frequency was 1.7 MHz, the pulsing imaging sequence used was power modulation (PM) with a mechanical index (MI) of less than 0.06, and the frame rate varied between 7 and 10 Hz. The acquisition mode was dual-contrast imaging and 2-min loops were acquired. During the acquisition, the focus was set

TABLE I. EXAMPLE OF SCORES RECEIVED BY VARIOUS STRUCTURES SHOWN IN FIG. 5.

Structure index	$S_M$	$S_F$	$S_B$	$S$
1	2.27	0.89	0	0.00
2	5.68	0.85	0	0.00
3	1.40	1.04	0	0.00
4	24.25	1.65	1	0.90
5	8.61	2.21	1	0.61

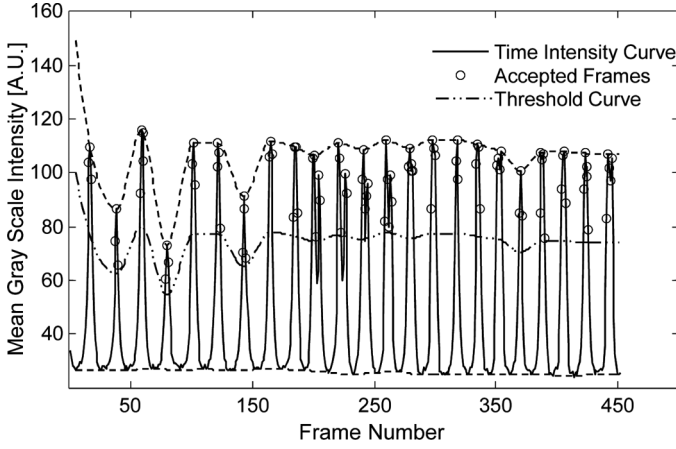


Fig. 7. Gated time-intensity curve (TIC) extracted from structure 4, shown in Fig. 5.

well below the depth of the lesion to ensure uniform pressure field. The time gain compensation (TGC) gain was adjusted in such a way that it was uniform across depth and avoided signal saturation. Before the arrival of the contrast agent, there was a hint of uniform noise in the image as an assurance that the TGC gain was at the threshold of detection.

A 2.4-mL bolus of Sonovue (Bracco s.p.a., Milan, Italy) was injected. The radiologist acquiring the loops maintained a constant imaging plane by observing the tissue side of the acquisition.

### C. Quantification Approach

The patient DICOM loops acquired with the Philips iU22 scanner were transferred to a workstation running the commercial quantification software QLAB (v. 8.1, Philips Medical Systems, Bothell, WA). An ROI was manually drawn on the trigger frame of the DCEUS loop encompassing the lesion (Fig. 9). Both the arterial and late portal phases of the DCEUS loop were used for the accurate drawing of the ROI [4].

Time-intensity curves from linearized image data were extracted using the QLAB software and saved to a text file. The B-mode loop image data, the trigger frame index, and the frame rate of the acquisition were also saved. This information was passed on to the Matlab implementation of the ARG algorithm. After processing by the ARG algorithm, a new lesion TIC was produced.

### D. Data Analysis

To assess the effectiveness of the ARG algorithm, both the TICs extracted with and without ARG processing were fitted on a lognormal indicator dilution model [8]. The goodness of fit of the data to the model was established using the coefficient of determination ( $R^2$ ) and the root mean square error (RMSE), shown in (8) and (9), respectively,

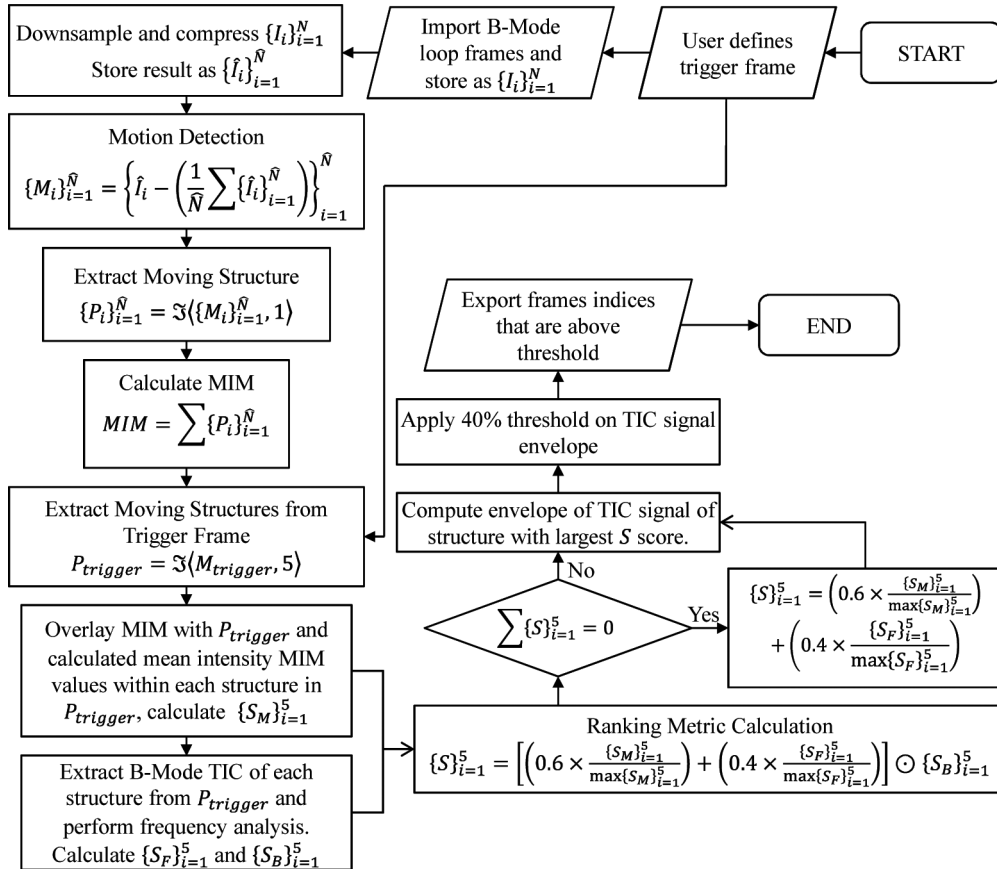


Fig. 8. Flowchart of the automatic respiratory gating (ARG) algorithm.



Fig. 9. Region of interest (ROI) drawn encompassing lesion on trigger frame of the dynamic contrast-enhanced ultrasound (DCEUS) loop, shown here in late portal phase. The mean linear intensity DCEUS values are extracted from within this ROI.

$$R^2 = 1 - \frac{\sum_i (y_i - f_i)^2}{\sum_i (y_i - \bar{y}_i)^2} \quad (8)$$

$$\text{RMSE} = \sqrt{\frac{\sum_{i=1}^n (y_i - f_i)^2}{n}}, \quad (9)$$

where  $y_i$  are the linear intensity data points,  $f_i$  are the corresponding points from the lognormal model fit,  $\bar{y}$  is the mean value of the  $y_i$  points, and  $n$  is the number of data points. An example of such an analysis is shown in Fig. 10.

To arrive at useful conclusions, the data were visualized as boxplots. The limits of the boxes are the 25% ( $Q_1$ ) and 75% ( $Q_3$ ) quartiles and the middle of the box indicates the median of the data. The lower limit of the whiskers is  $F_L = Q_1 - [1.5 \times (Q_3 - Q_1)]$  and the upper limit of the whiskers is  $F_U = Q_3 + [1.5 \times (Q_3 - Q_1)]$ . All data that are outside  $F_L$  and  $F_U$  are considered outliers. The boxplots have notches indicating 95% confidence intervals for the median, the limits of which are calculated as  $\text{median} \pm 1.57 \times (Q_3 - Q_1) / \sqrt{N}$ , where  $N$  is the number of samples.

Further to the boxplots of the data, one-tail paired  $t$ -tests with unequal variances were performed using the R programming language [17] and the pwr package [18] was used to calculate the power of the  $t$ -tests performed.

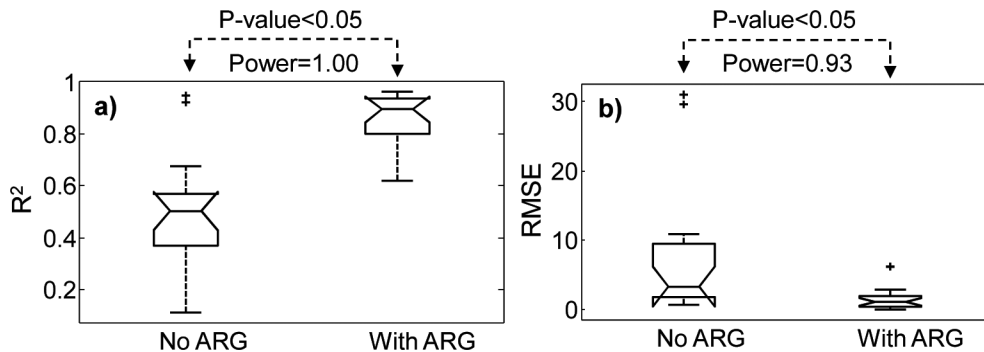


Fig. 11. (a) Boxplots of the  $R^2$  values and (b) boxplots of the root mean square error (RMSE) for the model fit of the clinical cases analyzed with and without automatic respiratory gating (ARG). The notches on the boxplots are the 95% confidence levels of the median. The  $p$ -values and the power at 95% confidence level of  $t$ -tests performed are also included.

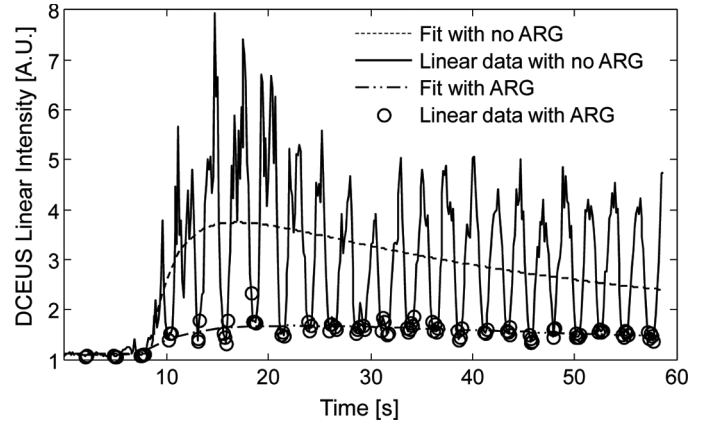


Fig. 10. Mean linear intensity data from a region of interest (ROI) around a lesion with and without automatic respiratory gating (ARG), including the fits on the lognormal indicator dilution model. In this example, the  $R^2$  of the fit with and without ARG are 0.89 and 0.37, respectively.

### III. RESULTS

The results of the  $t$ -test performed on the  $R^2$  with and without ARG processing show a  $p$ -value less than 0.05 with a  $t$ -test power of 1.00. A  $p$ -value of less than 0.05 is also calculated for the RMSE data with a  $t$ -test power of greater than 0.93. The  $p$ -values calculated and the powers of the tests allow for confident conclusions to be drawn from the analysis.

In Fig. 11 boxplots of the  $R^2$  and RMSE values of the lognormal model fits are plotted with and without ARG. From Fig. 11(a), it can be seen that the  $R^2$  95% confidence interval notches on the boxplots of with and without ARG processing are not overlapping. This is not the case, however, with the RMSE boxplot 95% confidence interval notches.

It should also be noted that the ARG algorithm, as implemented in Matlab 2007b, had a mean run time of  $0.87 \pm 0.10$  (standard deviation) seconds per 100 frames on an Intel E8400 (Intel Corp., Santa Clara, CA) at 3 GHz with 2 GB of RAM. These run times are faster than those previously published in the literature [11], [12], [15].

## IV. DISCUSSION

From Fig. 11, it is evident both from the notches on the boxplots and the  $t$ -test results that the  $R^2$  is indeed improved with the use of ARG, within a 95% confidence interval. However regarding the RMSE, although the  $t$ -test arrives at the conclusion that by using ARG the RMSE is significantly lower than without using ARG, there is an overlap of 1.2 RMSE units in the 95% confidence interval notches of the boxplots.

This mismatch is believed to be caused by the two outlier points seen clearly in Fig. 11(a) that have an  $R^2$  value, without the use ARG, of more than 0.8. In Fig. 12, the boxplots are redrawn, this time omitting the two outlier cases; note that the statistical power of the  $t$ -test on the RMSE data has increased, although marginally. Also note that the notches of the boxplots, in this case, do not overlap either for the  $R^2$  or RMSE boxplots. It is believed that certain patients' data do not suffer from respiratory motion as much as others even though, of course, there is respiratory motion present.

Another important assumption underlying this work is that a better fit of the data to the model suggests more accurate results on the hemodynamics of the lesion. This assumption considers respiratory motion as noise added to the data which, if removed, will provide more accurate results. However, it is very difficult to refer to "more accurate results" when the real perfusion of the lesion is unknown.

In addition to significantly increasing the goodness of fit of the lesion linear intensity data to the lognormal indicator dilution model, ARG results in effective frame downsampling by eliminating frames that are not useful for quantitative or qualitative evaluation. This frame downsampling makes the evaluation of the image loop faster by reducing the time required to calculate the fit of an indicator dilution model to the data, in the qualitative evaluation of the loop, and in parametric imaging approaches. The rejection of frames that are out of phase with the presence of the lesion on the imaging plane can also reduce the processing time for motion-compensation algorithms that use computing-intensive image processing techniques such as image registration [13]–[15].

For the goals of the current study, only a single phase of the breathing cycle was extracted by the ARG algorithm. However, there are clinical situations in which multiple breathing cycle phases must be extracted. An example of such a clinical situation is the presence of multiple lesions that cannot be captured on a single imaging plane. This multiphase extraction can be achieved using the ARG algorithm and modifying the gating of the lesion's TIC (Fig. 7) so that the signal envelope of the TIC is segmented into several parts, each representing a different breathing cycle phase.

This work concentrated on DCEUS of liver lesions but it should be noted that the ARG algorithm can be implemented in other DCEUS studies, such as the evaluation of blood flow in the hepatic artery and portal vein [19], [20]. Moreover, the ARG algorithm can also be used in conventional B-mode imaging to help with qualitative evaluation of video loops.

The novel algorithm presented addresses limitations of computational methods for compensation of respiratory motion found in the literature, such as the ability to select any breathing cycle phase desired by the clinician instead of extracting the end phases of the breathing cycle [11], [12]. The only user input required by the ARG algorithm is the trigger frame, whereas other methods in the literature require the user to draw ROIs on frames to perform rigid registration [13]–[15], a requirement that has the potential to introduce time delays in the clinical workflow.

Finally, it should be noted that the ARG algorithm cannot be applied in cases in which there was an accidental movement (by either the operator or the patient) that changed the image plane, unless the original image plane is recovered later in the loop. In such a case, the ARG algorithm will eliminate all motion frames acquired after the change of the imaging plane. Empirically, the minimum number of frames needed to perform a robust fit on the model lies between 100 and 150 frames for a 2-min acquisition.

## V. CONCLUSION

This study presents an ARG algorithm that can improve both the qualitative and quantitative analysis of

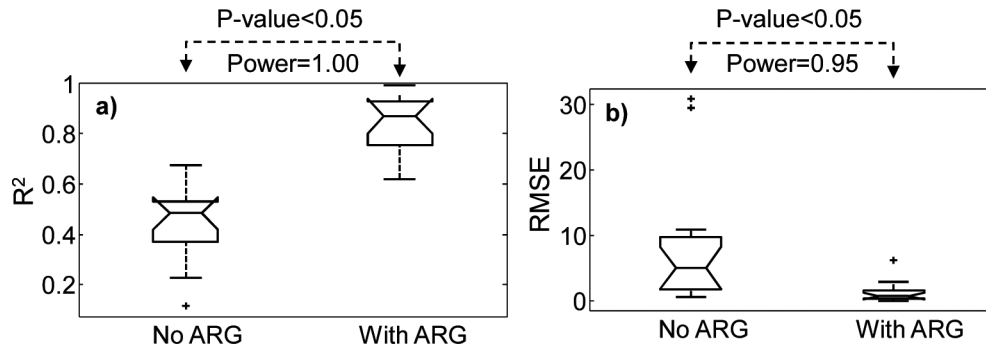


Fig. 12. (a) Boxplots of the  $R^2$  values and (b) boxplots of the root mean square error (RMSE) for the model fit of the clinical cases analyzed with and without ARG, not including the outlier cases. The notches on the boxplots are 95% confidence levels around the median. The  $p$ -values and the power at 95% confidence level of  $t$ -tests performed are also included.

DCEUS loops. The ARG algorithm requires only the selection of the trigger frame that defines the breathing cycle phase to be extracted and performs all other tasks automatically. The implementation of such algorithm is possible on any diagnostic ultrasound system that has a dual-contrast imaging mode. Furthermore, the patient is not required to alter his/her breathing, allowing for a comfortable examination. The effectiveness of the ARG algorithm in removing respiratory motion in a clinical setting has been demonstrated by the results of this study. Finally, this algorithm is very fast; it can remove respiratory motion from a 1000-frame loop in 8 s.

## REFERENCES

- [1] P. N. Burns, "Harmonic imaging with ultrasound contrast agents," *Clin. Radiol.*, vol. 51, suppl. 1, pp. 50–55, Feb. 1996.
- [2] M. Averkiou, M. Bruce, S. Jensen, P. Rafter, T. Brock-Fishe, and J. Powers, "Pulsing schemes for the detection of nonlinear echoes from contrast microbubbles," in *9th European Symp. Ultrasound Contrast Imaging*, 2004, pp. 17–24.
- [3] K. Wei, A. R. Jayaweera, S. Firoozan, A. Linka, D. M. Skyba, and S. Kaul, "Basis for detection of stenosis using venous administration of microbubbles during myocardial contrast echocardiography: Bolus or continuous infusion?" *J. Am. Coll. Cardiol.*, vol. 32, no. 1, pp. 252–260, Jul. 1998.
- [4] M. Averkiou, M. Lampaskis, K. Kyriakopoulou, D. Skarlos, G. Klouvas, C. Strouthos, and E. Leen, "Quantification of tumor microvasculature with respiratory gated contrast enhanced ultrasound for monitoring therapy," *Ultrasound Med. Biol.*, vol. 36, no. 1, pp. 68–77, Jan. 2010.
- [5] C. Huang-Wei, A. Bleuzen, P. Bourlier, J. Roumy, A. Bouakaz, L. Pourcelot, and F. Tranguart, "Differential diagnosis of focal nodular hyperplasia with quantitative parametric analysis in contrast-enhanced sonography," *Invest. Radiol.*, vol. 41, no. 3, pp. 363–368, Mar. 2006.
- [6] R. Senior, M. Monaghan, M. L. Main, J. L. Zamorano, K. Tiemann, L. Agati, N. J. Weissman, A. L. Klein, T. H. Marwick, M. Ahmad, A. N. DeMaria, M. Zabalgoitia, H. Becher, S. Kaul, J. E. Udelson, F. J. Wackers, R. C. Walovitch, and M. H. Picard, "Detection of coronary artery disease with perfusion stress echocardiography using a novel ultrasound imaging agent: Two Phase 3 international trials in comparison with radionuclide perfusion imaging," *Eur. J. Echocardiogr.*, vol. 10, no. 1, pp. 26–35, Jan. 2009.
- [7] L. Galiuto, B. Garramone, A. Scarà, A. G. Rebuzzi, F. Crea, G. La Torre, S. Funaro, M. Madonna, F. Fedele, and L. Agati, "The extent of microvascular damage during myocardial contrast echocardiography is superior to other known indexes of post-infarct reperfusion in predicting left ventricular remodeling," *J. Am. Coll. Cardiol.*, vol. 51, no. 5, pp. 552–559, Feb. 2008.
- [8] C. Strouthos, M. Lampaskis, V. Sboros, A. McNeilly, and M. Averkiou, "Indicator dilution models for the quantification of microvascular blood flow with bolus administration of ultrasound contrast agents," *IEEE Trans. Ultrason. Ferroelectr. Freq. Control*, vol. 57, no. 6, pp. 1296–1310, Jun. 2010.
- [9] H. S. Markus and M. J. Harrison, "Estimation of cerebrovascular reactivity using transcranial Doppler, including the use of breath-holding as the vasodilatory stimulus," *Stroke*, vol. 23, no. 5, pp. 668–673, May. 1992.
- [10] M. Müller, M. Voges, U. Piepgras, and K. Schimrigk, "Assessment of cerebral vasomotor reactivity by transcranial Doppler ultrasound and breath-holding. A comparison with acetazolamide as vasodilatory stimulus," *Stroke*, vol. 26, no. 1, pp. 96–100, Jan. 1995.
- [11] G. Renault, F. Tranguart, V. Perlberg, A. Bleuzen, A. Herment, and F. Frouin, "A posteriori respiratory gating in contrast ultrasound for assessment of hepatic perfusion," *Phys. Med. Biol.*, vol. 50, no. 19, pp. 4465–4480, Oct. 2005.
- [12] S. Mulé, N. Kachenoura, O. Lucidarme, A. De Oliveira, C. Pellot-Barakat, A. Herment, and F. Frouin, "An automatic respiratory gating method for the improvement of microcirculation evaluation: application to contrast-enhanced ultrasound studies of focal liver lesions," *Phys. Med. Biol.*, vol. 56, no. 16, pp. 5153–5165, Aug. 2011.
- [13] N. G. Rognin, M. Arditì, L. Mercier, P. J. A. Frinking, M. Schneider, G. Perrenoud, A. Anaye, J.-Y. Meuwly, and F. Tranguart, "Parametric imaging for characterizing focal liver lesions in contrast-enhanced ultrasound," *IEEE Trans. Ultrason. Ferroelectr. Freq. Control*, vol. 57, no. 11, pp. 2503–2511, Nov. 2010.
- [14] N. Rognin, R. Campos, J. Thiran, T. Messenger, P. Broillet, P. Frinking, M. Mercier, and M. Arditì, "A new approach for automatic motion compensation for improved estimation of perfusion quantification parameters in ultrasound imaging," in *8th French Conference on Acoustics*, 2006, pp. 61–65.
- [15] J. Zhang, M. Ding, F. Meng, M. Yuchi, and X. Zhang, "Respiratory motion correction in free-breathing ultrasound image sequence for quantification of hepatic perfusion," *Med. Phys.*, vol. 38, no. 8, pp. 4737–4748, Aug. 2011.
- [16] A. Jain, *Fundamentals of Digital Image Processing*. Englewood Cliffs, NJ: Prentice-Hall, 1989.
- [17] R Core Team. (2013, Oct.). R: A Language and Environment for Statistical Computing. [Online]. Available: <http://www.r-project.org>
- [18] S. Champely. (2013, Oct.). pwr: Basic functions for power analysis. [Online]. Available: <http://cran.r-project.org/web/packages/pwr/index.html>
- [19] T. P. Gauthier, A. Muhammad, H. S. Wasan, P. D. Abel, and E. L. S. Leen, "Reproducibility of quantitative assessment of altered hepatic hemodynamics with dynamic contrast-enhanced ultrasound," *J. Ultrasound Med.*, vol. 31, no. 9, pp. 1413–1420, Sep. 2012.
- [20] T. P. Gauthier, H. S. Wasan, A. Muhammad, D. R. Owen, and E. L. S. Leen, "Assessment of global liver blood flow with quantitative dynamic contrast-enhanced ultrasound," *J. Ultrasound Med.*, vol. 30, no. 3, pp. 379–385, Mar. 2011.



**Damianos Christofides** (S'13) was born in Limassol, Cyprus in 1981. He earned a B.Sc. degree in physics from Louisiana State University in 2005 and an M.Sc. degree in physics and computing in medicine and biology from the University of Manchester, UK, in 2006.

From 2006 to 2010, he worked as a Medical Physicist at the St. James's University Hospital in Leeds, UK, in the field of radiotherapy. He is currently pursuing a Ph.D. degree in mechanical engineering at the Biomedical Ultrasound Lab of the University of Cyprus. His current research interests include medical image processing and ultrasound contrast agent quantification.

Mr. Christofides is a registered Clinical Scientist by the Health and Care Professions Council (UK) and has been awarded the title of Chartered Scientist by the Science Council (UK). He has co-authored two papers in peer-reviewed journals and conference proceedings.

**Edward Leen's** photograph and biography were not available at time of publication.



**Michalakis Averkiou** (M'98–SM'11) received the B.S., M.S., and Ph.D. degrees in 1987, 1989, and 1994, respectively, all in mechanical engineering with specialization in nonlinear acoustics/biomedical ultrasound, from the University of Texas at Austin. He was a Postdoctoral Fellow at the Applied Physics Laboratory of the University of Washington from 1994 to 1996. He worked in the Philips Medical Systems R&D department from 1996 to 2005. He is currently an associate professor in the Department of Mechanical and Manufacturing Engineering of the University of Cyprus. His research interests are in the areas of ultrasound imaging, microbubble ultrasound contrast agents and their applications in oncology, quantification of tumor angiogenesis, therapeutic applications of ultrasound, and ultrasound-induced drug delivery.